

# Unveiling the Hidden Realm: Self-supervised Skeleton-based Action Recognition in Occluded Environments

Yifei Chen<sup>1</sup>, Kunyu Peng<sup>1,\*</sup>, Alina Roitberg<sup>2</sup>, David Schneider<sup>1</sup>, Jiaming Zhang<sup>1</sup>, Junwei Zheng<sup>1</sup>, Ruiping Liu<sup>1</sup>, Yufan Chen<sup>1</sup>, Kailun Yang<sup>3,4</sup>, and Rainer Stiefelhagen<sup>1</sup>

**Abstract**—To integrate action recognition methods into autonomous robotic systems, it is crucial to consider adverse situations involving target *occlusions*. Such a scenario, despite its practical relevance, is rarely addressed in existing self-supervised skeleton-based action recognition methods. To empower robots with the capacity to address occlusion, we propose a simple and effective method. We first pre-train using occluded skeleton sequences, then use k-means clustering (KMeans) on sequence embeddings to group semantically similar samples. Next, we employ K-nearest-neighbor (KNN) to fill in missing skeleton data based on the closest sample neighbors. Imputing incomplete skeleton sequences to create relatively complete sequences as input provides significant benefits to existing skeleton-based self-supervised models. Meanwhile, building on the state-of-the-art Partial Spatio-Temporal Learning (PSTL), we introduce an Occluded Partial Spatio-Temporal Learning (OPSTL) framework. This enhancement utilizes Adaptive Spatial Masking (ASM) for better use of high-quality, intact skeletons. The effectiveness of our imputation methods is verified on the challenging occluded versions of the NTURGB+D 60 and NTURGB+D 120. The source code will be made publicly available at <https://github.com/cyfml/OPSTL>.

## I. INTRODUCTION

Human action recognition has extensive applications in the field of robotics, such as human-robot interaction, healthcare, industrial automation, security, and surveillance [1]–[5]. In particular, robots can collaborate with humans as partners, assist them in various tasks by identifying human actions and needs, and take care of patients. The capability to understand human intentions and goals allows a robot to discern when its assistance is most needed, thereby minimizing disruptions to human activities. A robot equipped with a human action recognition system can also be used to monitor the condition of patients to provide better daily-life assistance for their recovery [6], [7], assess the safety of its surroundings, issue warnings, and detect gestures for help in rescue missions to provide assistance. Challenges of image- or video-based

This work was supported in part by the SmartAge project sponsored by the Carl Zeiss Stiftung (P2019-01-003; 2021-2026), the MWK through the Cooperative Graduate School Accessibility through AI-based Assistive Technology (KATE) under Grant BW6-03, and in part by the BMBF through a fellowship within the IFI program of the German Academic Exchange Service (DAAD), in part by the HoreKA@KIT supercomputer partition, and in part by Hangzhou SurImage Technology Company Ltd.

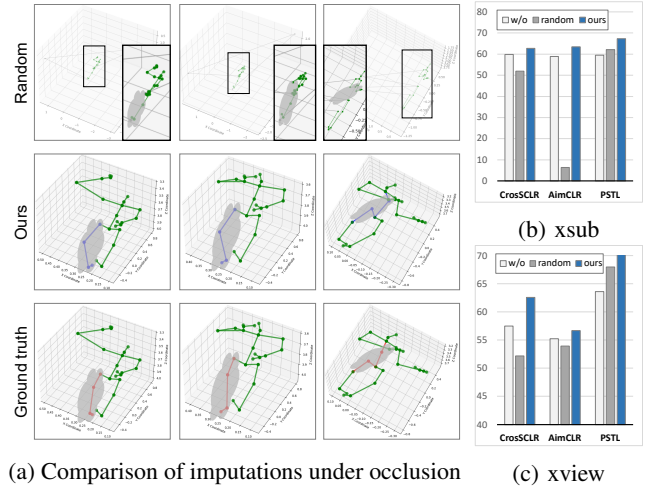
\*Corresponding author. (Email: kunyu.peng@kit.edu.)

<sup>1</sup>The authors are the Institute for Anthropomatics and Robotics, Karlsruhe Institute of Technology, Germany.

<sup>2</sup>The author is with the Institute for Artificial Intelligence, University of Stuttgart, Germany.

<sup>3</sup>The author is with the School of Robotics, Hunan University, China.

<sup>4</sup>The author is also with the National Engineering Research Center of Robot Visual Perception and Control Technology, Hunan University, China.



(a) Comparison of imputations under occlusion (b) xsub (c) xvview

Fig. 1: Comparison of different imputation methods. In (a), we compare random imputations (in gray), our imputation results (in blue), and ground-truth skeletons (in red). In (b) and (c), the linear evaluation results of cross-subject (*xsub*) and cross-view (*xvview*) settings are tested by using imputation methods across three popular self-supervised action recognition methods (CrossCLR, AimCLR, and PSTL).

action recognition [8] stem from multiple factors: complex backgrounds, variations in human body shapes, changing viewpoints, or motion speed alterations. In contrast to video-based action recognition [9]–[11], skeleton-based action recognition is less sensitive to appearance factors and has the advantage of superior efficiency by using sparse 3D skeleton data as input, which ensures fast inference speed and small memory usage. Thanks to the advancement of depth sensors [12] and lightweight and robust pose estimation algorithms [13], [14], obtaining high-quality skeleton data is becoming easier. Skeleton-based action recognition has rapidly progressed in recent years. Its efficiency designates it for mobile robots with computational constraints, at the same time self-supervised solutions [15], [16] have gradually grasped the attention of the robot research community since this technique allows for training such methods with little annotation effort.

The majority of existing work on self-supervised skeleton-based action recognition [17]–[19] is conducted on occlusion-free data collected in well-constrained environments. In practice, robots often encounter occluded environments in the real world, even high-quality pose detectors can not provide reliable full-body poses in such situations. For this reason, we argue that occlusion-aware training and

evaluation is an overlooked but crucial task in this field. The occlusion problem in self-supervised skeleton-based action recognition can be considered from two points of view. On one hand, it can be addressed by improving the robustness of the model to occlusion by manipulating the model architecture, and on the other hand, it can be handled through the data itself and completing the missing skeleton coordinates as much as possible.

In this work, we for the first time tackle the self-supervised skeleton-based action recognition task under occlusions. A benchmark is firstly built by introducing the occlusion derived from Peng *et al.* [20]. On this benchmark, obvious performance decays are observed when using occluded skeleton data on all existing methods. We thereby contribute a new method by considering both model- and data perspectives, and then evaluate the proposed solution on this benchmark. From the model perspective, we introduce a novel dataset-driven *Adaptive Spatial Masking (ASM)* data augmentation based on the current state-of-the-art approach, *i.e.*, PSTL [21]. This method masks joints based on the distribution of missing joints within the dataset to effectively leverage intact data to learn feature representation. For the data-driven approach, we propose a simple but effective method that enhances the performance of existing popular self-supervised action recognition methods for downstream tasks by completing missing data, as shown in Fig. 1. Intuitively, one might search for similar dataset samples to fill in missing data. However, due to the vast amount of data and the density of the original skeleton data, directly applying KNN [22] to search for neighboring samples is highly impractical and unacceptable in terms of both time and space considerations. To improve computational efficiency, we propose a two-stage approach. In the first stage, samples are grouped into distinct categories through KMeans [23] clustering on features learned through self-supervised learning methods. In the second stage, missing values are imputed by leveraging close neighbors within the same cluster.

The proposed approach eliminates the need for a KNN search on the entire dataset during the imputation process. Instead, KNN imputation is applied within each smaller cluster, leading to a considerable reduction in computational overhead. We summarize our contributions as follows:

- To investigate robotic action recognition performance in difficult environments, a large-scale occlusion-based benchmark is constructed for self-supervised skeleton-based action recognition, including both NTU-60 and NTU-120 datasets.
- We propose a two-stage imputation method using KMeans and KNN to reduce computation overhead for the occluded skeleton completion. Our approach is flexible and applicable to various methods for self-supervised skeleton-based action recognition.
- We present the *Occluded Partial Spatio-Temporal Learning (OPSTL)* framework to better leverage high-quality skeleton data by a novel dataset-driven *Adaptive Spatial Masking (ASM)* data augmentation.

- We verify the effectiveness of our method with extensive experiments on the occluded version of NTU-60 and NTU-120 datasets.

## II. RELATED WORK

### A. Skeleton-based Action Recognition

Early existing approaches for skeleton-based action recognition primarily concentrated on developing hand-crafted features [24], [25]. With the rapid advancement of deep learning, early deep-learning methods included transforming skeleton data into images and utilizing convolutional neural networks (CNNs) [26]–[28] for resolution, as well as directly utilizing recurrent neural networks (RNNs) [29]–[31] to process skeleton data. ST-GCN [32] initially proposed to treat skeleton data as pre-defined graphs and use graph convolutional neural networks (GCN) to aggregate information between joints. Subsequently, various methods based on ST-GCN have been continuously introduced, such as GCNs with attention mechanisms and multi-stream GCNs [33]–[35]. In this paper, existing popular methods all adopt ST-GCN as the backbone for feature extraction.

### B. Self-supervised Representation Learning

In the early stages of self-supervised learning, novel pretext tasks were designed to generate supervision from the inherent characteristics of the data itself, *e.g.*, jigsaw puzzles [36], [37], colorization [38], and predicting rotation [39], [40]. However, their performance heavily relies on the design of pretext tasks, and the generalization performance to downstream tasks cannot be guaranteed. Then, Instance discrimination-based contrastive learning methods, *e.g.*, MOCO and MOCOv2 [41], [42], utilize queue-based memory banks to store a large number of negative samples and employ momentum updating mechanisms. Additionally, SimCLR [43] computes embeddings in real time using larger batch sizes. They all require a substantial number of negative samples for contrastive learning. Therefore, negative-sample-free methods like BYOL [44], SimSiam [45], and Barlow Twins [46] have been proposed to break free from the constraint of requiring a large number of negative samples for contrastive learning. Recently, MAE [47] has been introduced for learning informative visual representations through the utilization of local complementary information.

### C. Self-supervised Skeleton-based Action Recognition

LongT GAN [48] uses an encoder-decoder structure to regenerate the input sequence, yielding valuable feature representations. Meanwhile, P&C [49] creates a weaker decoder, forcing the encoder to learn more discriminative features. MS2L [17] introduces a multi-task self-supervised learning framework involving motion predictions and jigsaw puzzles. AS-CAL [50] and SkeletonCLR [18] utilize momentum updates in contrastive learning on individual streams. However, CrosSCLR [18] goes beyond single-stream considerations. It employs a cross-view knowledge mining strategy to facilitate knowledge sharing between different streams, aiming to extract more valuable information. AimCLR [19] recognizes

the significance of data augmentation in contrastive learning and thus explores a multitude of data augmentation methods and combines them. On the other hand, PSTL [21] uses a spatiotemporal masking strategy to learn more generalized representations from partial skeleton sequences. In this work, we first construct a large-scale self-supervised skeleton-based action recognition benchmark considering existing well-established self-supervised skeleton-based action recognition approaches under realistic occlusion from [20] and then propose an *Occluded Partial Spatio-Temporal Learning* (OPSTL) framework by using ASM and skeleton-based imputation, simultaneously.

### III. METHODOLOGY

Our method, *i.e.*, OPSTL, is based on PSTL [21] due to its superior performance in comparison to other approaches when handling occlusions. The Central Spatial Masking (CSM) of PSTL is replaced by our Adaptive Spatial Masking (ASM) to better handle occlusion in the first self-supervised training phase (first stage). Occlusions are handled through data imputation before the second self-supervised training phase, where embedding clusters obtained after the first stage training and KNN are leveraged (second stage), as shown in Fig. 2. KMeans divides embeddings into smaller clusters. Subsequently, data imputation is performed using KNN search to find samples that are similar to the ones needing completion. Note that, the data imputation method in the second stage can be used on all self-supervised skeleton-based action recognition methods. After imputing the missing data, downstream tasks can achieve improvements compared with occluded data using the same self-supervised skeleton-based action recognition method.

#### A. Pre-processing

A pre-processed skeleton sequence can be represented as  $s \in \mathbb{R}^{C \times T \times V}$  from the original input  $I \in \mathbb{R}^{C \times T \times V \times M}$ .  $T$  is the frame number and  $V$  is the joint number.  $C$  denotes the channel number.  $M$  represents the person number. The preprocessing is similar to that of CrosSCLR [18]. Skeleton coordinates are relative coordinates, relative to the center joint of the skeleton. Additionally, we need to compute the missing joint boolean matrix ( $\mathbf{B} \in \mathbb{B}^{N \times V}$ ) of the  $V$  joints for each sample to better mask the joints that are more occluded in the Adaptive Spatial Masking (ASM). The coordinates of all missing joints will be represented as “nan”, which facilitates the subsequent calculation of Euclidean distances with missing values during imputation.

#### B. Partial Spatio-Temporal Skeleton Representation Learning

Many existing methods [18], [19] focus on generating various views of skeleton sequences for contrastive learning, but they often overlook the local relationships between different skeleton joints and frames. However, these local relationships are vital for real-world applications because they provide critical context for tasks like action recognition. To bridge this

gap, Partial Spatio-Temporal Learning (PSTL) [21] leverages local relationships by using a unique spatiotemporal masking strategy to create partial skeleton sequences. These sequences are utilized in a triplet stream structure comprising an anchor stream, a spatial masking stream with Central Spatial Masking (CSM), and a temporal masking stream with Motion Attention Temporal Masking (MATM). Therefore, PSTL shows a certain level of effectiveness in handling occlusion. PSTL adopts the framework of Barlow Twins [46], thus avoiding the drawbacks of contrastive learning that require a large number of negative samples, as well as the need for a large batch size and memory bank [18], [19].

#### C. Adaptive Spatial Masking

The self-supervised skeleton-based action recognition method, PSTL [21], employs Central Spatial Masking (CSM) to enhance the robustness of the learned representation with respect to joints. CSM promotes generating similar features from partial skeleton data and whole skeleton data, enabling the encoder to learn the relationship between masked and unmasked joints. CSM selects joints to be masked based on the degree of centrality of the human skeleton graph topology because the joints with more degrees can acquire richer neighborhood information. The joints with higher degrees are more likely to be masked. Joints’ masked probability is defined as:

$$p_i = \frac{d_i}{\sum_{j=1}^n d_j}, \quad (1)$$

$d_i$  is the degree of each joint  $v_i$ .

However, it does not take into account considering the actual occlusion situation. When only some joints of each sample are occluded, we can choose to mask the joints with higher occlusion frequency in the training set to better utilize high-quality data for learning. On the other hand, when each sample is randomly occluded with a higher occlusion rate, the masking strategy should also shift from a fixed strategy to a random mask, in order to better simulate the distribution of occlusions. Therefore, we propose dataset-driven Adaptive Spatial Masking (ASM), which can adaptively switch between partial occlusion and random occlusion. It is worth noting that we still retain CSM in ASM. When no joints are occluded in this batch, we still use CSM to select joints for masking. We redefine the degree of each joint based on the missing joint boolean matrix ( $\mathbf{B}$ ) in each batch. The missing frequency of each joint  $v_i, i \in (1, 2, \dots, n)$  is calculated within each batch. The frequency degree (FD) of joint  $v_i$  can be formulated as:

$$FD_i = \lfloor \frac{F_i - \min(F)}{\max(F) - \min(F) + \epsilon} \times 3 + 1 \rfloor, \quad (2)$$

where  $\epsilon$  is a small value of 0.001. We observed that the majority of joints have a degree of around 2, and the differences in degrees are relatively small. Consequently, the performance difference between random masking and degree-based masking is not significant. Thus, we rescale the frequency of each joint’s occlusion to a range similar to the degrees, *i.e.*, [1, 3]. Due to the larger differences

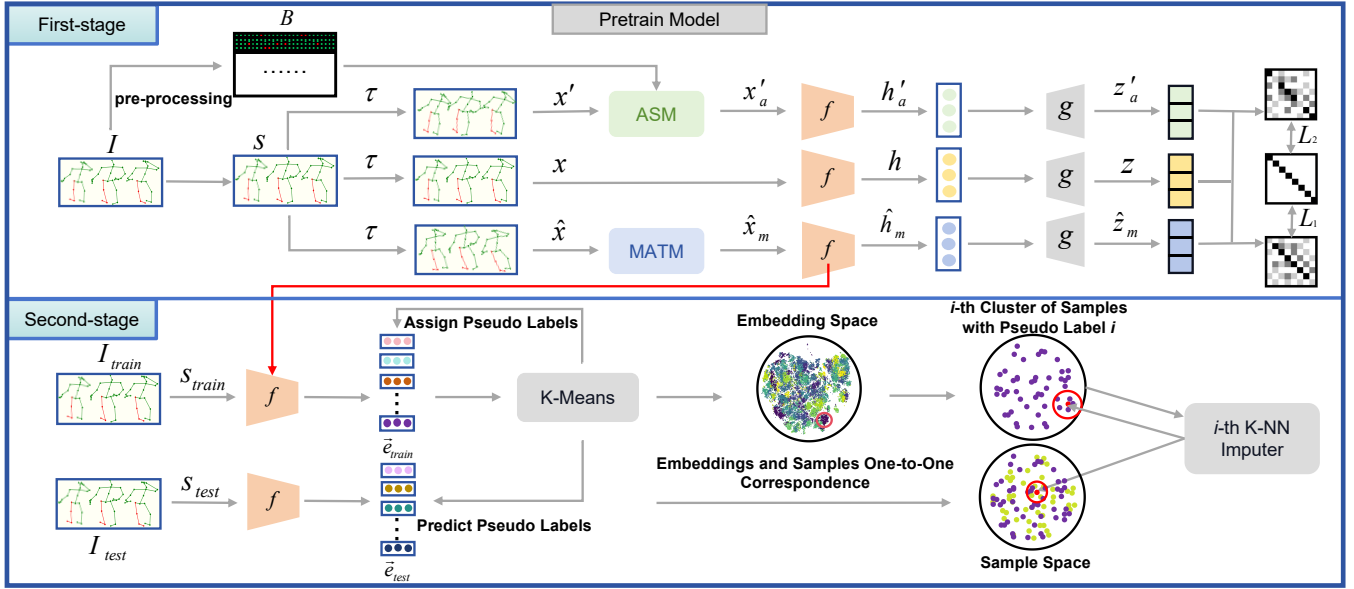


Fig. 2: Our two-stage method for completing missing skeleton coordinates. The red portion in input  $I$  represents the missing skeleton. In the first stage, the pre-training model adopts the PSTL framework, with CSM replaced by ASM, to better utilize high-quality data. The second stage involves completing the entire dataset by partitioning samples into smaller clusters using KMeans. Subsequently, the KNN-imputer is employed to find neighboring samples and complete the missing coordinates. Yellow points in the sample space are samples from the test set, and purple points are samples from the training set.

in frequency degrees generated by this rescaling compared to the degree of centrality of the human skeleton graph topology, the joint masking tends to favor joints with a higher frequency of occlusion. Here  $F$  is the frequency of missing joints computed on  $B$  along the batch dimension  $b$ :

$$F_i = \sum_b B_{b,i}. \quad (3)$$

#### D. Imputation

Inspired by traditional machine learning-based KNN imputation, we aim to find the most similar samples to the ones with missing values for imputation. However, due to the high dimensionality and large amount of sample data, directly searching for neighbors in the sample space is impractical. Therefore, we consider it unnecessary to search the entire sample space. Instead, we divide the samples into clusters with fewer skeleton samples. Through the first stage of pre-training, KMeans can roughly cluster samples with the same action type into a cluster.

Firstly, we need to use the pre-trained model from the first stage to extract features from the samples. The extracted embeddings  $\vec{e}_{train} \in \mathbf{R}^{N \times D}$ , where  $N$  is the number of samples in the training set and  $D$  is the dimension of embeddings, are clustered using KMeans, and pseudo-labels are assigned to each embedding. Since there is a one-to-one correspondence between embeddings and original samples, each sample is also assigned a pseudo-label. For a given cluster of samples with pseudo label  $i$ , we utilize KNN to search for neighboring samples of the sample that need imputation within the same cluster. Because these neighboring samples may also have missing values, the standard Euclidean distance is not applicable. Here, we use a modified Euclidean distance based on missing values [51], [52], which

is formulated as:

$$\text{dist}(S_{ij}, S_{ik}) = \sqrt{w \times d_{\text{ignore}}(S_{ij}, S_{ik})}, \quad (4)$$

where  $w$  is a weight that can be expressed as the ratio of the total number of coordinates to the number of present coordinates, and  $d_{\text{ignore}}(S_{ij}, S_{ik})$  is the Euclidean distance between sample  $j$  and sample  $k$  in  $i$ -th cluster that ignores missing values in  $S_{ij}$  and  $S_{ik}$ .

Based on this distance metric, it is straightforward to compute distances between each pair of samples. The nearest  $k$  samples  $S_{ij}^{\text{near}}$ ,  $j \in (1, 2, \dots, k)$  are selected based on distance and missing position from the current cluster  $i$  for one of the samples with missing data  $S_i^{\text{miss}}$ , and each sample  $S_{ij}^{\text{near}}$  should have intact coordinate  $C_j$  at the position  $p \in \mathbb{Z}^{T \times V \times M}$  where missing coordinates  $C_i^{\text{miss}} = \{c \mid c \in S_i^{\text{miss}}\}$  occur. The imputation formula for a missing skeleton coordinate of a missing sample is given as:

$$C_m^{\text{miss}} = \frac{\sum_{j=1}^k r_j \times C_j}{\sum_{j=1}^k r_j}, m \in (1, 2, \dots, n), \quad (5)$$

where  $r_j$  is the reciprocal of the modified Euclidean distance, denoted by  $\text{dist}$ , between a missing sample  $S_{im'}^{\text{miss}}$ ,  $m' \in (1, 2, \dots, n)$  and one of nearest  $k$  samples  $S_{ij}^{\text{near}}$ :

$$r_j = \frac{1}{\text{dist}(S_{ij}, S_{im'}^{\text{miss}})}. \quad (6)$$

As shown in Fig. 2, the difference between the imputation of the training set and the test set is that we don't recluster the test set from scratch. Instead, the KMeans model trained on the training set is used to predict pseudo-labels for the test set. The imputed data is then generated using clusters from the training set that share the same pseudo-labels as



those predicted for the test set. The test set is solely utilized as a source of data requiring imputation.

While this approach has shown improvements in various downstream tasks across multiple models, there are still limitations. When certain joints of all data in a cluster are missing, the missing parts cannot be imputed. Therefore, it does not guarantee the complete imputation of all missing skeleton coordinates.

## IV. EXPERIMENTS

### A. Datasets

**NTU-RGB+D 60/120 with occlusion.** The occluded datasets are derived from NTU-60/120. The NTU-60 dataset [53] was captured by using Microsoft Kinect sensors and comprises 56,578 skeleton sequences involving 60 distinct action categories. There are two splits [53]: 1) Cross-Subject (xsub): training data and validation data are captured from different subjects. 2) Cross-View (xview): training data and validation data are captured from different camera views. NTU-120 dataset [54] is the extended version of the NTU-60, which comprises 113,945 skeleton sequences involving 120 action categories. NTU-120 keeps the xsub protocol while using xset protocol to evaluate with different camera setups instead of views. There are two types of occlusions: 1) Synthesized realistic occlusion [20], which leverages 3D furniture projections to generate realistic occlusions. 2) Random occlusion, which is according to the minimum and maximum values of the coordinates, where 20% of the coordinates are randomly selected for occlusion.

### B. Protocols

**Linear Evaluation Protocol.** To elaborate, we train a supervised linear classifier consisting of a fully connected layer followed by a softmax layer while keeping the encoder fixed. **Semi-supervised Evaluation Protocol.** We initially pre-train the encoder using the entire imputed dataset and subsequently fine-tune the complete model using only 1% or 10% randomly chosen labeled data.

**Finetune Protocol.** We attach a linear classifier to the trained encoder and finetune the entire network on the imputed data.

### C. Implementation Details

In our experiments, all pre-trained models are based on ST-GCN [32] with 16 hidden channels as the backbone. For training, we employ the Adam optimizer [55] and use the CosineAnnealing scheduler with a total of 150 epochs for both representation learning and downstream tasks. Our batch size is set to 128. The learning rate is set to  $5e-3$ .

**Data Augmentation.** Data augmentation is performed to diversify skeleton sequences before feature extraction during model training. Each model uses its specific set of data augmentation methods. For instance, SkeletonCLR and CrosSCLR utilize one spatial augmentation (Shear) and one temporal augmentation (Crop). PSTL uses three spatial augmentations (Shear, Rotate, Spatial Flip) and one temporal augmentation (Crop). Our OPSTL uses the same data augmentation method as PSTL.

**Self-supervised Pre-training.** To ensure a direct comparison with PSTL, we use the same set of parameters. As shown in Fig. 2, the incomplete skeleton sequence  $S$  through transformation  $\tau$  has three different views  $x, x', \hat{x}$ .  $x'$  and  $\hat{x}$  pass through ASM and MATM to create partial skeleton sequence  $x'_a, \hat{x}_m$ . ST-GCN is used as the backbone  $f$  to extract 256-dimensional features  $h, h'_a, \hat{h}_m$ , which are then projected to 6144-dimensional embeddings  $z, z'_a, \hat{z}_m$  through projector  $g$ . To capture the relationship between masked joints and unmasked ones, we compute the cross-correlation matrix between embeddings  $z$  and  $z'_a$ , as well as  $z$  and  $\hat{z}_m$ .  $L1$  and  $L2$  are calculated using the two cross-correlation matrices. The loss parameter  $\lambda$  is set to  $2e^{-4}$ , and a warm-up strategy of 10 training epochs is applied. Weight decay is set to  $1e^{-5}$ . For ASM, 9 joints are masked, and for MATM, 10 frames are masked.

**Imputation.** We proposed an imputation method to deal with occlusion. For clustering during imputation, we employ KMeans with 60 clusters for NTU-60 and 120 clusters for NTU-120 with realistic occlusions. We use KNN with a value of  $k$  set to 5 to search for neighboring samples in the imputation process.

### D. Comparison with Non-imputed NTU-60/120

To demonstrate the effectiveness of our imputation method, we compare it with the non-imputed NTU-60/120 with realistic occlusion. As shown in Tables I, II, and III, almost all three downstream task performances of all the investigated methods have shown improvements on the imputed NTU-60/120 dataset.

TABLE I: Linear evaluation results on **NTU-60** with synthesized realistic occlusion, randomly imputed values, and imputed values by our proposed method. “ $\Delta$ ” represents the difference compared to the non-imputed NTU-60. **J** and **M** represent the joint stream and the motion stream.

Method	Stream	Occluded (%)		Randomly imputed (%)				Our imputed (%)			
		xsub acc.	xview acc.	xsub acc.	$\Delta$	xview acc.	$\Delta$	xsub acc.	$\Delta$	xview acc.	$\Delta$
SkeletonCLR [18]	<b>J</b>	56.74	53.25	47.12	$\downarrow 9.62$	58.09	$\uparrow 4.84$	57.61	$\uparrow 0.87$	64.43	$\uparrow 11.18$
2s-CrosSCLR [18]	<b>J+M</b>	59.88	57.47	51.96	$\downarrow 7.92$	52.18	$\downarrow 5.29$	62.76	$\uparrow 2.88$	62.54	$\uparrow 5.07$
AimCLR [19]	<b>J</b>	58.90	55.21	6.36	$\downarrow 52.54$	53.91	$\downarrow 1.30$	63.40	$\uparrow 4.50$	56.68	$\uparrow 1.47$
PSTL [21]	<b>J</b>	59.52	63.60	62.18	$\uparrow 2.66$	67.97	$\uparrow 4.37$	<b>67.31</b>	$\uparrow 7.79$	71.10	$\uparrow 7.50$
<b>OPSTL (ours)</b>	<b>J</b>	<b>61.11</b>	<b>65.55</b>	<b>65.63</b>	$\uparrow 4.52$	<b>68.01</b>	$\uparrow 2.46$	67.11	<b>66.00</b>	<b>71.39</b>	$\uparrow 5.84$

TABLE II: Linear evaluation results on **NTU-120** with synthesized realistic occlusion, randomly imputed values, and imputed values by our proposed method. “ $\Delta$ ” represents the difference compared to the non-imputed NTU-120. **J** and **M** represent the joint stream and the motion stream.

Method	Stream	Occluded (%)		Randomly imputed (%)				Our imputed (%)			
		xsub acc.	xset acc.	xsub acc.	$\Delta$	xset acc.	$\Delta$	xsub acc.	$\Delta$	xset acc.	$\Delta$
SkeletonCLR [18]	<b>J</b>	44.93	42.78	44.42	$\downarrow 0.51$	40.12	$\downarrow 4.66$	48.63	$\uparrow 3.70$	45.06	$\uparrow 2.28$
2s-CrosSCLR [18]	<b>J+M</b>	49.63	48.14	39.11	$\downarrow 10.52$	33.77	$\downarrow 14.37$	49.58	$\downarrow 0.05$	54.43	$\uparrow 6.29$
AimCLR [19]	<b>J</b>	44.58	48.93	0.86	$\downarrow 43.72$	1.16	$\downarrow 47.77$	52.50	$\uparrow 7.92$	52.83	$\uparrow 3.90$
PSTL [21]	<b>J</b>	54.18	51.90	56.12	$\uparrow 1.94$	52.66	$\uparrow 0.76$	57.05	$\uparrow 2.87$	57.94	$\uparrow 6.04$
<b>OPSTL (ours)</b>	<b>J</b>	<b>55.65</b>	<b>54.18</b>	<b>56.43</b>	$\uparrow 0.78$	<b>53.90</b>	$\downarrow 0.28$	<b>59.29</b>	$\uparrow 3.64$	<b>58.25</b>	$\uparrow 4.07$

TABLE III: Finetune and Semi-supervised results on the imputed NTU-60/120 with synthesized realistic occlusion. “ $\Delta$ ” represents the difference compared to the non-imputed NTU-60/120 with synthesized realistic occlusion. **J** and **M** represent the joint stream and the motion stream.

Method	Stream	Imputed NTU-60 (%)				Imputed NTU-120 (%)			
		xsub acc.	$\Delta$	xview acc.	$\Delta$	xsub acc.	$\Delta$	xset acc.	$\Delta$
<b>Finetune:</b>									
SkeletonCLR [18]	J	70.58	$\uparrow 3.22$	80.76	$\uparrow 4.42$	63.17	$\uparrow 4.06$	62.12	$\uparrow 1.20$
2s-CrosSCLR [18]	J+M	72.94	$\uparrow 1.32$	80.34	$\uparrow 0.09$	65.06	$\uparrow 0.39$	67.45	$\uparrow 2.43$
AimCLR [19]	J	70.53	$\uparrow 0.44$	75.52	$\downarrow 3.21$	67.08	$\uparrow 5.25$	66.62	$\uparrow 1.91$
PSTL [21]	J	75.16	$\uparrow 2.48$	85.24	$\uparrow 2.05$	69.10	$\uparrow 1.20$	69.42	$\uparrow 2.71$
OPSTL (ours)	J	<b>75.43</b>	$\uparrow 2.41$	<b>86.01</b>	$\uparrow 1.92$	<b>70.89</b>	$\uparrow 2.21$	69.14	$\uparrow 1.89$
<b>Semi 1%:</b>									
SkeletonCLR [18]	J	31.99	$\uparrow 13.47$	31.18	$\uparrow 10.16$	20.45	$\uparrow 3.13$	16.24	$\uparrow 2.23$
2s-CrosSCLR [18]	J+M	32.66	$\uparrow 4.69$	31.18	$\uparrow 10.35$	19.38	$\uparrow 0.21$	20.12	$\uparrow 7.59$
AimCLR [19]	J	34.44	$\uparrow 5.28$	27.04	$\uparrow 8.92$	22.59	$\uparrow 6.13$	20.68	$\uparrow 5.38$
PSTL [21]	J	<b>40.81</b>	$\uparrow 7.99$	<b>39.61</b>	$\uparrow 13.06$	27.43	$\uparrow 5.92$	<b>25.52</b>	$\uparrow 6.52$
OPSTL (ours)	J	40.07	$\uparrow 6.48$	38.65	$\uparrow 10.76$	<b>27.90</b>	$\uparrow 4.69$	24.57	$\uparrow 4.71$
<b>Semi 10%:</b>									
SkeletonCLR [18]	J	55.97	$\uparrow 2.98$	60.83	$\uparrow 9.37$	44.37	$\uparrow 2.33$	42.68	$\uparrow 7.72$
2s-CrosSCLR [18]	J+M	59.17	$\uparrow 3.16$	59.01	$\uparrow 3.86$	46.89	$\uparrow 2.07$	48.24	$\uparrow 8.44$
AimCLR [19]	J	59.64	$\uparrow 2.30$	54.34	$\downarrow 0.36$	48.38	$\uparrow 6.25$	48.96	$\uparrow 3.63$
PSTL [21]	J	63.04	$\uparrow 4.41$	68.89	$\uparrow 7.54$	53.26	$\uparrow 2.80$	53.42	$\uparrow 4.14$
OPSTL (ours)	J	<b>64.04</b>	$\uparrow 5.26$	<b>70.04</b>	$\uparrow 6.22$	<b>54.71</b>	$\uparrow 2.90$	<b>53.50</b>	$\uparrow 3.38$

### E. Comparison with State-of-the-art

We conduct a series of comparison experiments to evaluate OPSTL. As shown in Tables I, II, and III, for all the non-imputed, randomly imputed, and imputed NTU-60/120, OPSTL outperforms the current state-of-the-art method PSTL on linear evaluation. OPSTL is improved by 1.59% and 1.95% on xsub and xview of NTU-60 with realistic occlusion, respectively. In addition, OPSTL achieves a performance gain of 1.47% and 2.28% on xsub and xset of NTU-120 with realistic occlusion. OPSTL achieves not only improvements on the non-imputed dataset but also on the imputed NTU-60/120 dataset.

### F. Ablation Study

We conduct ablation experiments to demonstrate the effectiveness of the proposed adaptive Spatial Masking (ASM) and imputation method.

1) To validate the effectiveness of the imputation method, we perform random imputation on NTU-60/120 with realistic occlusion. From Table I and Table II, it is obvious that our proposed imputation method outperforms random imputation on linear evaluation. The performances of SkeletonCLR, 2s-CrosSCLR, and AimCLR all deteriorate under random imputation. The most severe decline is observed in AimCLR, where the accuracy drops to nearly 1%. This clearly illustrates that random completion undermines the whole skeleton information, which is crucial for action recognition methods that leverage whole skeleton data.

On the contrary, in the case of methods that utilize partial skeleton sequences for representation learning, such as PSTL, there is still a slight improvement in accuracy despite the use of random imputation. However, for our proposed ASM, the improvement is minimal or even negative. For instance, on xset of randomly imputed NTU-120, OPSTL experiences a reduction of 0.28% in accuracy compared to

TABLE IV: Stepwise ablation results on realistic occluded and imputed NTU-120. Method<sup>1+2</sup> denotes two stages during the pre-training. **S1** is first stage and **S2** is second stage. All experiments are on the joint stream.

Method <sup>1+2</sup>	(S1) Occluded NTU-120 (%)		(S2) Imputed NTU-120 (%)	
	xsub	xset	xsub	xset
PSTL [21] + PSTL [21]	54.18	51.90	57.05	57.94
OPSTL (ours) + PSTL [21]	55.65	54.18	58.70	57.52
<b>OPSTL (ours) + OPSTL (ours)</b>	<b>55.65</b>	<b>54.18</b>	<b>59.29</b>	<b>58.25</b>

non-imputed data. Yet, it still outperforms the state-of-the-art PSTL. This observation underscores the fact ASM effectively utilizes high-quality data for representation learning.

2) To better illustrate the effectiveness of ASM, we conducted a stepwise ablation study on the NTU-120 dataset. As shown in Table IV, during the first stage of pre-training, we observed that using ASM yields accuracy improvements of 1.47% for xsub and 2.28% for xset over CSM. Building upon the ASM-based first stage, in the second stage, both CSM and ASM are employed. The results indicate in the second stage, continuing to use ASM yields gains of 0.59% for xsub and 0.73% for xset compared to using CSM.

3) To demonstrate the effectiveness of our imputation method on random occlusions, we validate it using OPSTL on the NTU-60/120 datasets. As shown in Table V, after the imputation, OPSTL exhibits significant improvements across various splits of the NTU-60/120 datasets.

TABLE V: Linear evaluation results of OPSTL on non-imputed and imputed NTU-60/120 with random occlusion. All experiments are on the joint stream.

Method	Randomly occluded NTU-60 (%)		Randomly occluded NTU-120 (%)	
	xsub	xview	xsub	xset
Non-Imputed	41.90	30.16	10.32	4.22
Imputed	47.31	55.29	23.54	18.59

## V. CONCLUSION

In this paper, we propose effective solutions for the challenges of self-supervised skeleton-based action recognition in occluded environments. First, we construct a large-scale occluded self-supervised skeleton-based human action recognition benchmark considering well-established approaches and propose the Adaptive Spatial Masking (ASM) data augmentation mechanism. We introduce a two-stage skeleton data imputation method using KMeans and KNN, reducing computation overhead for occluded skeleton completion. The Occluded Partial Spatio-Temporal Learning (OPSTL) framework integrates these methods effectively. Experimental results validate the efficacy of our approach across various self-supervised approaches, empowering robots to perform robust action recognition in real-world occluded scenarios.

## REFERENCES

- [1] C. Bandi and U. Thomas, "Skeleton-based action recognition for human-robot interaction using self-attention mechanism," in *2021 16th IEEE International Conference on Automatic Face and Gesture Recognition (FG)*, 2021, pp. 1–8.
- [2] Z. Song *et al.*, "Attention-oriented action recognition for real-time human-robot interaction," in *2020 International Conference on Pattern Recognition (ICPR)*, 2020, pp. 7087–7094.
- [3] A. Sharghi, H. Haugerud, D. Oh, and O. Mohareri, "Automatic operating room surgical activity recognition for robot-assisted surgery," in *International Conference on Medical Image Computing and Computer Assisted Intervention (MICCAI)*, 2020, pp. 385–395.
- [4] V. Voronin, M. Zhdanova, E. Semenishchev, A. Zelenskii, Y. Cen, and S. Agaian, "Action recognition for the robotics and manufacturing automation using 3-D binary micro-block difference," *The International Journal of Advanced Manufacturing Technology*, vol. 117, pp. 2319–2330, 2021.
- [5] S. Danafar and N. Gheissari, "Action recognition for surveillance applications using optic flow and svm," in *Computer Vision—ACCV 2007: 8th Asian Conference on Computer Vision, Tokyo, Japan, November 18–22, 2007, Proceedings, Part II 8*. Springer, 2007, pp. 457–466.
- [6] A. Sabater, L. Santos, J. Santos-Victor, A. Bernardino, L. Montesano, and A. C. Murillo, "One-shot action recognition in challenging therapy scenarios," in *2021 IEEE/CVF Conference on Computer Vision and Pattern Recognition Workshops (CVPRW)*, 2021, pp. 2771–2779.
- [7] H. Yan, B. Hu, G. Chen, and E. Zhengyuan, "Real-time continuous human rehabilitation action recognition using OpenPose and FCN," in *2020 3rd International Conference on Advanced Electronic Materials, Computers and Software Engineering (AEMCSE)*, 2020, pp. 239–242.
- [8] M. B. Shaikh and D. Chai, "RGB-D data-based action recognition: A review," *Sensors*, vol. 21, no. 12, p. 4246, 2021.
- [9] K. Simonyan and A. Zisserman, "Two-stream convolutional networks for action recognition in videos," in *Advances in Neural Information Processing Systems (NeurIPS)*, vol. 27, 2014, pp. 568–576.
- [10] A. Ullah, J. Ahmad, K. Muhammad, M. Sajjad, and S. W. Baik, "Action recognition in video sequences using deep bi-directional LSTM with CNN features," *IEEE Access*, vol. 6, pp. 1155–1166, 2017.
- [11] H. H. Pham, L. Khoudour, A. Cruzil, P. Zegers, and S. A. Velastin, "Video-based human action recognition using deep learning: A review," *arXiv preprint arXiv:2208.03775*, 2022.
- [12] Z. Zhang, "Microsoft kinect sensor and its effect," *IEEE MultiMedia*, vol. 19, no. 2, pp. 4–10, 2012.
- [13] Z. Cao, T. Simon, S.-E. Wei, and Y. Sheikh, "Realtime multi-person 2D pose estimation using part affinity fields," in *2017 IEEE Conference on Computer Vision and Pattern Recognition (CVPR)*, 2017, pp. 1302–1310.
- [14] G. Hua, H. Liu, W. Li, Q. Zhang, R. Ding, and X. Xu, "Weakly-supervised 3D human pose estimation with cross-view U-shaped graph convolutional network," *IEEE Transactions on Multimedia*, vol. 25, pp. 1832–1843, 2023.
- [15] X. Liu *et al.*, "Self-supervised learning: Generative or contrastive," *IEEE Transactions on Knowledge and Data Engineering*, vol. 35, no. 1, pp. 857–876, 2023.
- [16] G. Kahn, A. Villaflor, B. Ding, P. Abbeel, and S. Levine, "Self-supervised deep reinforcement learning with generalized computation graphs for robot navigation," in *2018 IEEE International Conference on Robotics and Automation (ICRA)*, 2018, pp. 5129–5136.
- [17] L. Lin, S. Song, W. Yang, and J. Liu, "MS2L: Multi-task self-supervised learning for skeleton based action recognition," in *ACM International Conference on Multimedia (MM)*, 2020, pp. 2490–2498.
- [18] L. Li, M. Wang, B. Ni, H. Wang, J. Yang, and W. Zhang, "3D human action representation learning via cross-view consistency pursuit," in *2021 IEEE/CVF Conference on Computer Vision and Pattern Recognition (CVPR)*, 2021, pp. 4741–4750.
- [19] T. Guo, H. Liu, Z. Chen, M. Liu, T. Wang, and R. Ding, "Contrastive learning from extremely augmented skeleton sequences for self-supervised action recognition," in *AAAI Conference on Artificial Intelligence (AAAI)*, vol. 36, no. 1, 2022, pp. 762–770.
- [20] K. Peng, A. Roitberg, K. Yang, J. Zhang, and R. Stiefelhagen, "Delving deep into one-shot skeleton-based action recognition with diverse occlusions," *IEEE Transactions on Multimedia*, vol. 25, pp. 1489–1504, 2023.
- [21] Y. Zhou, H. Duan, A. Rao, B. Su, and J. Wang, "Self-supervised action representation learning from partial spatio-temporal skeleton sequences," in *AAAI Conference on Artificial Intelligence (AAAI)*, 2023, pp. 3825–3833.
- [22] T. M. Cover and P. E. Hart, "Nearest neighbor pattern classification," *IEEE Transactions on Information Theory*, vol. 13, no. 1, pp. 21–27, 1967.
- [23] T. Kanungo, D. M. Mount, N. S. Netanyahu, C. D. Piatko, R. Silverman, and A. Y. Wu, "An efficient k-means clustering algorithm: analysis and implementation," *IEEE Transactions on Pattern Analysis and Machine Intelligence*, vol. 24, no. 7, pp. 881–892, 2002.
- [24] R. Vemulapalli, F. Arrate, and R. Chellappa, "Human action recognition by representing 3D skeletons as points in a lie group," in *2014 IEEE Conference on Computer Vision and Pattern Recognition (CVPR)*, 2014, pp. 588–595.
- [25] L. Xia, C.-C. Chen, and J. K. Aggarwal, "View invariant human action recognition using histograms of 3D joints," in *2012 IEEE Conference on Computer Vision and Pattern Recognition Workshops (CVPRW)*, 2012, pp. 20–27.
- [26] Y. Du, Y. Fu, and L. Wang, "Skeleton based action recognition with convolutional neural network," in *2015 IAPR Asian Conference on Pattern Recognition (ACPR)*, 2015, pp. 579–583.
- [27] Q. Ke, M. Bennamoun, S. An, F. Sohel, and F. Boussaid, "A new representation of skeleton sequences for 3D action recognition," in *2017 IEEE Conference on Computer Vision and Pattern Recognition (CVPR)*, 2017, pp. 4570–4579.
- [28] M. Liu, H. Liu, and C. Chen, "Enhanced skeleton visualization for view invariant human action recognition," *Pattern Recognition*, vol. 68, pp. 346–362, 2017.
- [29] Y. Du, W. Wang, and L. Wang, "Hierarchical recurrent neural network for skeleton based action recognition," in *2015 IEEE Conference on Computer Vision and Pattern Recognition (CVPR)*, 2015, pp. 1110–1118.
- [30] S. Song, C. Lan, J. Xing, W. Zeng, and J. Liu, "Spatio-temporal attention-based LSTM networks for 3D action recognition and detection," *IEEE Transactions on Image Processing*, vol. 27, no. 7, pp. 3459–3471, 2018.
- [31] P. Zhang, C. Lan, J. Xing, W. Zeng, J. Xue, and N. Zheng, "View adaptive neural networks for high performance skeleton-based human action recognition," *IEEE Transactions on Pattern Analysis and Machine Intelligence*, vol. 41, no. 8, pp. 1963–1978, 2019.
- [32] S. Yan, Y. Xiong, and D. Lin, "Spatial temporal graph convolutional networks for skeleton-based action recognition," in *AAAI Conference on Artificial Intelligence (AAAI)*, vol. 32, no. 1, 2018.
- [33] L. Shi, Y. Zhang, J. Cheng, and H. Lu, "Two-stream adaptive graph convolutional networks for skeleton-based action recognition," in *2019 IEEE/CVF Conference on Computer Vision and Pattern Recognition (CVPR)*, 2019, pp. 12018–12027.
- [34] C. Si, W. Chen, W. Wang, L. Wang, and T. Tan, "An attention enhanced graph convolutional LSTM network for skeleton-based action recognition," in *2019 IEEE/CVF Conference on Computer Vision and Pattern Recognition (CVPR)*, 2019, pp. 1227–1236.
- [35] Z. Chen, S. Li, B. Yang, Q. Li, and H. Liu, "Multi-scale spatial temporal graph convolutional network for skeleton-based action recognition," in *AAAI Conference on Artificial Intelligence (AAAI)*, vol. 35, no. 2, 2021, pp. 1113–1122.
- [36] M. Noroozi, A. Vinjimoor, P. Favaro, and H. Pirsivash, "Boosting self-supervised learning via knowledge transfer," in *2018 IEEE/CVF Conference on Computer Vision and Pattern Recognition (CVPR)*, 2018, pp. 9359–9367.
- [37] C. Wei *et al.*, "Iterative reorganization with weak spatial constraints: Solving arbitrary jigsaw puzzles for unsupervised representation learning," in *2019 IEEE/CVF Conference on Computer Vision and Pattern Recognition (CVPR)*, 2019, pp. 1910–1919.
- [38] R. Zhang, P. Isola, and A. A. Efros, "Colorful image colorization," in *European Conference on Computer Vision (ECCV)*, vol. 9907, 2016, pp. 649–666.
- [39] X. Zhai, A. Oliver, A. Kolesnikov, and L. Beyer, "S4L: Self-supervised semi-supervised learning," in *2019 IEEE/CVF International Conference on Computer Vision (ICCV)*, 2019, pp. 1476–1485.
- [40] S. Gidaris, P. Singh, and N. Komodakis, "Unsupervised representation learning by predicting image rotations," in *International Conference on Learning Representations (ICLR)*, 2018.
- [41] K. He, H. Fan, Y. Wu, S. Xie, and R. Girshick, "Momentum contrast for unsupervised visual representation learning," in *2020 IEEE/CVF*

- Conference on Computer Vision and Pattern Recognition (CVPR)*, 2020, pp. 9726–9735.
- [42] X. Chen, H. Fan, R. Girshick, and K. He, “Improved baselines with momentum contrastive learning,” *arXiv preprint arXiv:2003.04297*, 2020.
- [43] T. Chen, S. Kornblith, M. Norouzi, and G. Hinton, “A simple framework for contrastive learning of visual representations,” in *International Conference on Machine Learning (ICML)*, 2020, pp. 1597–1607.
- [44] J.-B. Grill *et al.*, “Bootstrap your own latent—a new approach to self-supervised learning,” in *Advances in Neural Information Processing Systems (NeurIPS)*, vol. 33, 2020, pp. 21 271–21 284.
- [45] X. Chen and K. He, “Exploring simple siamese representation learning,” in *2021 IEEE/CVF Conference on Computer Vision and Pattern Recognition (CVPR)*, 2021, pp. 15 745–15 753.
- [46] J. Zbontar, L. Jing, I. Misra, Y. LeCun, and S. Deny, “Barlow twins: Self-supervised learning via redundancy reduction,” in *International Conference on Machine Learning (ICML)*, vol. 139, 2021, pp. 12 310–12 320.
- [47] K. He, X. Chen, S. Xie, Y. Li, P. Dollár, and R. B. Girshick, “Masked autoencoders are scalable vision learners,” in *2021 IEEE/CVF Conference on Computer Vision and Pattern Recognition (CVPR)*, 2021, pp. 15 979–15 988.
- [48] N. Zheng, J. Wen, R. Liu, L. Long, J. Dai, and Z. Gong, “Unsupervised representation learning with long-term dynamics for skeleton based action recognition,” in *AAAI Conference on Artificial Intelligence (AAAI)*, vol. 32, no. 1, 2018.
- [49] K. Su, X. Liu, and E. Shlizerman, “Predict & cluster: Unsupervised skeleton based action recognition,” in *2020 IEEE/CVF Conference on Computer Vision and Pattern Recognition (CVPR)*, 2020, pp. 9628–9637.
- [50] H. Rao, S. Xu, X. Hu, J. Cheng, and B. Hu, “Augmented skeleton based contrastive action learning with momentum LSTM for unsupervised action recognition,” *Information Sciences*, vol. 569, pp. 90–109, 2021.
- [51] J. K. Dixon, “Pattern recognition with partly missing data,” *IEEE Transactions on Systems, Man, and Cybernetics*, vol. 9, no. 10, pp. 617–621, 1979.
- [52] F. Pedregosa *et al.*, “Scikit-learn: Machine learning in python,” *Journal of Machine Learning Research*, vol. 12, pp. 2825–2830, 2011.
- [53] A. Shahroudy, J. Liu, T.-T. Ng, and G. Wang, “NTU RGB+ D: A large scale dataset for 3D human activity analysis,” in *2016 IEEE Conference on Computer Vision and Pattern Recognition (CVPR)*, 2016, pp. 1010–1019.
- [54] J. Liu, A. Shahroudy, M. Perez, G. Wang, L.-Y. Duan, and A. C. Kot, “NTU RGB+D 120: A large-scale benchmark for 3D human activity understanding,” *IEEE Transactions on Pattern Analysis and Machine Intelligence*, vol. 42, no. 10, pp. 2684–2701, 2020.
- [55] D. P. Kingma and J. Ba, “Adam: A method for stochastic optimization,” in *International Conference on Learning Representations (ICLR)*, 2015.